Pergamon

Chemical Engineering Science, Vol. 52, No. 13, pp. 2185–2196, 1997

Printed in Great Britain
PII: S0009-2509(97)00044-4
0009-2509/97 $17.00 + 0.00

Boundary element techniques for efficient 2-D and 3-D electrical impedance tomography

Ramani Duraiswami,* Georges L. Chahine and Kausik Sarkar
Dynaflow, Inc., 7210 Pindell School Road, Fulton, MD 20759, U.S.A.

(Received 19 March 1996; in revised form 28 August 1996; accepted 25 September 1996)

Abstract—This paper presents applications of boundary element methods to electrical impedance tomography. An algorithm for imaging the interior of a domain that consists of regions of constant conductivity is developed, that makes use of a simpler parametrization of the shapes of the regions to achieve efficiency. Numerical results from tests of this algorithm on synthetic data are presented, and show that the method is quite promising. © 1997 Elsevier Science Ltd. All rights reserved

Keywords: Electrical impedance tomography; boundary element method; inverse problem.

1. INTRODUCTION

In electrical impedance tomography (EIT) the distribution of impedances inside an object ('image') is sought by applying specified currents at some electrodes, and performing measurements of the voltage at other electrodes. The equations for the electric field then provide a relationship between the impedance distribution inside the medium and the measured voltages and applied currents. Different kinds of materials have different impedances, and the availability of an impedance map provides an image of the material distribution. EIT provides an exciting possibility for low-cost imaging, as it uses relatively inexpensive electricity sources for the probing in contrast to the other imaging techniques that rely on nuclear or X-ray radiation or difficult to construct magnetic elements. Since the mid-1980s, EIT has seen intense research efforts to develop it into a useful technique for medical and process imaging, and significant progress has been made on the modeling, implementation and use of the technique (Holder, 1993, Quinto *et al.*, 1994).

Impedance tomography techniques are indirect, in that the image must be deduced from measurements of some quantities which must then be transformed and interpreted to obtain the required image. Achieving this image requires the solution of a non-linear inverse problem, which can only be solved by using iterative techniques. The iterative algorithm for reconstruction as implemented in our study is summarized as follows:

1. Assume a conductivity distribution.
2. Using this distribution, and the applied currents, predict the voltage at the measurement electrodes. This is called the *forward problem.*
3. Compare the predicted voltages with the measured values, and determine the error between the measurement and the prediction.
4. Stop if the error is below a specified tolerance. Otherwise generate a new guess of the conductivity distribution using an error minimization procedure, and repeat the iterative steps.

This is illustrated in Fig. 1. The inverse problem is known to be ill-posed (e.g. see Somersalo *et al.*, 1992). As a consequence, the reconstruction procedure is sensitive to external noise and unless the reconstruction procedure regularizes the solution one can get images of poor quality. Further, classical schemes based on the finite element method (FEM) are often very time consuming, and require extensive computational resources. This is especially so for three-dimensional problems where these requirements can make them time-consuming from an operational viewpoint.

This has led to the wide use of backprojection methods to obtain the image (Barber and Brown, 1984), which are based on the idea that the sought image is a perturbation of a known configuration. However, the backprojection methods are restricted to particular geometries, often provide only qualitative images, and become quite inaccurate when there are large variations of the conductivity in the domain being imaged (Yorkey, 1987; Santosa and Vogelius, 1990).

*Corresponding author.

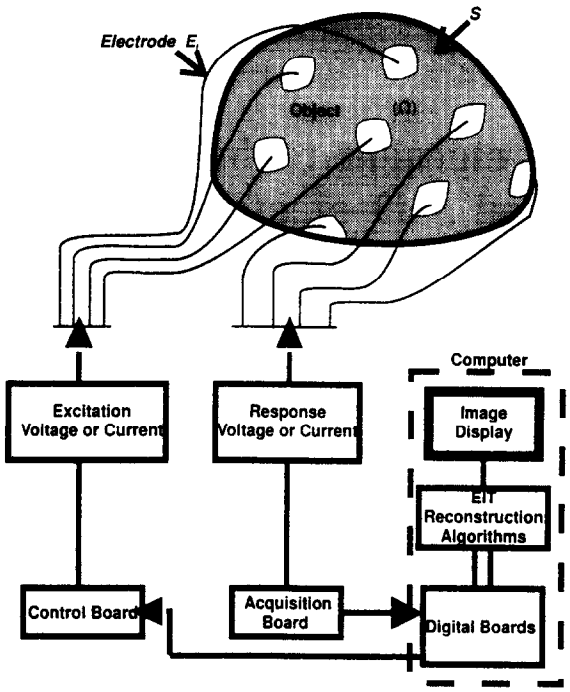

Fig. 1. Notations and operational concept of an EIT experiment.

1.1. *Approach*

Even though our approach applies to the general problem (Duraiswami *et al.*, 1995, 1996), in this paper we restrict ourselves to the problem where the domain to be imaged consists of regions of vanishing conductivity embedded in a domain of constant conductivity. Such problems arise quite often in practice (e.g. imaging gas bubbles in a host liquid or imaging cracks in a conducting material). The goal of the tomography in this case is to determine the shape of the interface of the embedded regions. In ongoing work we are investigating solution of more general tomography problems using dual reciprocity BEM techniques.

1.1.1. *Forward problem.* Previous investigators have used the finite-element method (FEM) for solving the forward problem. The FEM technique requires discretization of the whole domain into elements, with which are associated unknown values of electric potential. Accuracy requires that a large number of elements/variables be used for the discretization. For complex distribution of materials or in three-dimensional problems, a very large number of unknowns is therefore required, and the solution of the forward problem becomes computationally intensive. To increase the efficiency of the solution of the forward problem we employed boundary element methods (BEM).

These methods convert the field equations to integral equations posed on the boundary of the domain, and effectively reduce the dimension of the numerical problem. Only the boundaries of the domain need to be discretized, resulting in a considerable reduction in the number of variables required for accurate solution. The task of meshing the domain is also simplified.

1.1.2. *Inverse problem.* The solution of the inverse problem, requires 'parameterization' of the impedance, i.e. the distribution of impedance must be represented in terms of a set of parameters. Specification of these parameters determines the impedance shape distribution. The solution of the inverse problem then consists of determining these parameters. Typically, in FEM-based approaches, a simple parameterization related to the discretization is used, and the conductivity is treated as unknown on each element. This results in a huge minimization problem. Further, new estimates of the conductivity at each iteration require the complete evaluation of the FEM matrices each time the forward problem is to be solved. These factors make the solution of the inverse problem computationally intensive. To reduce the size of the inverse problem we use simpler parameterizations of the unknown conductivities that utilize available *a priori* knowledge about the problem.

2. GOVERNING EQUATIONS

Let us consider an electrical impedance tomography problem where we know the current at the whole outside boundary of the domain, and the voltage at selected points on the boundary. We have N_E different current patterns applied using M different electrodes. The current flowing out of the domain in between the electrodes is taken to be zero. The

electrical potential at the electrodes is also available. Our objective is to obtain σ, the distribution of conductivity in the material.

The electric potential, ϕ, satisfies the following equation where $\mathbf{n}$ is the boundary normal:

$$\nabla\cdot(\sigma\nabla\phi)=0 \quad \text{in } \Omega \tag{1}$$

$$\text{subject to} \begin{cases} \dfrac{\partial\phi}{\partial n} \text{ and } \phi \text{ known at the electrodes} \\ \dfrac{\partial\phi}{\partial n}=0 \text{ on the rest of the boundary.} \end{cases} \tag{2}$$

2.1. *Simplified equations for constant conductivity regions*

Often the sample to be imaged consists of regions of almost constant conductivity, σ_1, embedded in a continuous phase of another almost constant conductivity, σ_2 (e.g. spatial phase distribution: solid, liquid, or gas). In this case, the goal of the imaging is to determine the shape of the interfaces S_{int}. Since the conductivity is practically constant within each of the materials, the field equation reduces to

$$\nabla^2\phi_i=0 \quad \text{in } \Omega, \quad i=1,2. \tag{3}$$

The boundary conditions at the outer surface are given by eq. (2). We must, however, add the conditions of continuity of the potential and flux at the unknown interface(s) S_{int},

$$\phi_1|_{S_{\text{int}}}=\phi_2|_{S_{\text{int}}}, \qquad \sigma_1\frac{\partial\phi_1}{\partial n}\bigg|_{S_{\text{int}}}=\sigma_2\frac{\partial\phi_2}{\partial n}\bigg|_{S_{\text{int}}}. \tag{4}$$

In these problems, the forward problem consists of the solution of the Laplace equation in each medium, the solutions being coupled by boundary conditions of the form (4).

An additional important simplification arises if the interfaces to be imaged enclose materials of vanishing conductivity. Such situations are common in practice, e.g. in determining the distribution of air bubbles in a liquid, or cracks in a structure. In this special case, the boundary conditions (4) simplify to

$$\frac{\partial\phi}{\partial n}=0 \quad \text{on } S_{\text{int}}. \tag{5}$$

It is important to mention that these interface determination problems are ones that traditional FEM-based EIT methods find very difficult to solve since FEM does not explicitly treat the unknown interface, but accounts for it as a region of strong variation of the conductivity.

3. NUMERICAL FORMULATION

3.1. *Forward problem solution using BEM techniques*

Being able to solve an EIT problem using the BEM would have the invaluable advantage of considerably reducing computational time. Indeed, by requiring discretization of only the boundary, the BEM reduces the dimension of the problem by one, and leads to orders of magnitude reduction in memory and CPU time requirements.

Let us denote the fundamental solution to Laplace's equation by G, so that

$$\nabla^2 G(\mathbf{x},\mathbf{y})=\begin{cases}2\pi\delta(\mathbf{x}-\mathbf{y}) & \text{in 2-D}\\ 4\pi\delta(\mathbf{x}-\mathbf{y}) & \text{in 3-D}\end{cases}$$

$$\text{where } G=\begin{cases}\log|\mathbf{x}-\mathbf{y}| & \text{in 2-D}\\ -|\mathbf{x}-\mathbf{y}|^{-1} & \text{in 3-D.}\end{cases} \tag{6}$$

Equations (1) and (3) can all be reformulated via Green's identity:

$$a\pi\phi(\mathbf{x})=\int_V \nabla^2\phi(\mathbf{y})G(\mathbf{x},\mathbf{y})\,dV+\int_S \mathbf{n}_y\cdot[\phi(\mathbf{y})\nabla G(\mathbf{x},\mathbf{y}) - G(\mathbf{x},\mathbf{y})\nabla\phi(\mathbf{y})]\,dS \tag{7}$$

where $a\pi$ is the angle in two-dimensions (solid angle in three-dimensions) under which the point $\mathbf{x}$ sees the rest of the domain. For formulations with smooth boundaries we have

$$a=\begin{cases}2, & \mathbf{x}\in\Omega \text{ in 2-D}\\ 4, & \mathbf{x}\in\Omega \text{ in 3-D}\end{cases} \qquad a=\begin{cases}1, & \mathbf{x}\in S \text{ in 2-D}\\ 2, & \mathbf{x}\in S \text{ in 3-D}\end{cases}$$

where Ω is the domain, and S its boundary.

When we restrict ourselves to problems with internal regions of vanishing conductivity, the volume integral in eq. (7) vanishes. The surface integrals can then be performed by suitably discretizing the boundaries. In two-dimensions, we accomplish this by fitting cubic splines through known points on the boundary, while in three-dimension, we use plane triangular discretizations of the boundary. This enables us to write Green's identity in the form

$$a\pi\phi(\mathbf{x})=\sum_{k=1}^{N}\int_{S_k}\left(\phi(\mathbf{y})\frac{\partial G}{\partial n_y}(\mathbf{x},\mathbf{y})-G(\mathbf{x},\mathbf{y})\times\frac{\partial\phi}{\partial n_y}(\mathbf{y})\right)dS_k. \tag{8}$$

Over each subdomain S_k, a linear Lagrangian interpolation of ϕ and $\partial\phi/\partial n$ is performed using the values at the nodes (spline-knots in two-dimensions, triangle vertices in three-dimensions). The resultant boundary integrals can then be performed, leading to a discrete relation between the values of ϕ at points $\mathbf{x}$, and the values of ϕ and $\partial\phi/\partial n$ on the boundary nodes. Following a collocation approach, by selecting the points $\mathbf{x}$ to be the nodes on S, a linear system of equations of the form

$$\mathbf{A}\frac{\partial\phi}{\partial\mathbf{n}}=\mathbf{B}\phi \tag{9}$$

results. Here, $\mathbf{A}$ and $\mathbf{B}$ are matrices corresponding to the discretization and integration with Green's function and its derivative. On accounting for boundary conditions at the collocation points, one obtains a closed system of equations, which leads to ϕ and $\partial\phi/\partial n$ at the boundary. Knowing these quantities, eq. (7) can be used to obtain ϕ at any other point $\mathbf{x}$.

The process of discretization, evaluation of the normals, performance of integrations (including special cases that are singular when the collocation node lies in the interval of integration) is an involved process, and details may be found in Chahine and Perdue (1989) and Chahine and Duraiswami (1992, 1994).

3.2. *The inverse problem*

3.2.1. *Decoupled parameterization.* In our approach, we have decoupled the parameterization of the unknown conductivity or surface location from the forward problem discretization. This leads to a significant reduction of the number of parameters in the inverse problem, through use of *a priori* information about the physical problem at hand. This has also the advantage of mitigating the ill-posed character of the problem.

3.2.1.1. Parametrizations chosen for this study

For preliminary testing of our codes we chose the standard two-dimensional problems of identifying a cylindrical object inside a cylindrical container, on the boundary of which electric measurements are taken. In this case we parameterized the inner circle by the location of its center, and by its radius (three parameters). The codes were then tested for multiple circles in the inner domain. We then considered single and multiple regions of arbitrary shapes that are each described by a series of Legendre polynomials

$$f(r, \theta) = \sum_{k=0}^{N} r_k P_k(\cos\theta) \tag{10}$$

where in addition to N Legendre parameters, the direction to measure the angle θ and the origin of coordinates of the shape, lead to a total of $N+3$ parameters. For the three-dimensional codes we considered as a test problem a spherical container with internal regions consisting of single or multiple spheres of vanishing conductivity. The choice of circular and spherical container is purely for convenience of the setup of the problem, and the codes in their present form are written for any user prescribed shape of the boundary.

3.2.2. *Objective function for minimization.* The quantity to be imaged, here the shape of the regions of zero conductivity, are described through a parameterization by P quantities, arranged in the vector $\mathbf{P}$. To formulate an error function for minimization, we consider N_E different experiments, where in each experiment the pattern of current application to the electrodes is varied. The correct solution to the problem, $\phi^{(k)}$, satisfies the following boundary conditions at the M electrodes for $k = 1, \ldots, N_E$:

$$\sigma \frac{\partial \phi^{(k)}}{\partial n} = g^{(k)} \quad \text{on } S$$

and

$$\phi^{(k)} = \hat{\phi}^{(k)} \quad \text{on } E_l; \quad l = 1, \ldots, M \tag{11}$$

where the superscript k refers to a given experiment, E_l to electrode l, $\hat{\phi}^{(k)}$ refers to the measurements available at the electrodes.

The numerical solution of the forward problem, $\phi^{(k)}$, obtained by using the boundary conditions on the current provides us with a predicted value of the potential, $\tilde{\phi}$ at the electrodes

$$\phi^{(k)} = \tilde{\phi}_l^{(k)} \quad \text{on } E_l, \quad l = 1, \ldots, M. \tag{12}$$

We can accordingly form $M \times N_E$ measures of the error, e,

$$e_i = \hat{\phi}_l^{(k)} - \tilde{\phi}_l^{(k)}, \qquad i = 1, \ldots, MN_E. \tag{13}$$

We seek the values of $\mathbf{p}$ that minimize the above vector of errors. The classical technique for minimizing an array of objectives is to use a least-squares approach, which reduces them to a single objective function. The least-squares objective function can be formulated as

$$\chi^2 = \sum_{i=1}^{M \times N_E} [\hat{\phi}_i - \tilde{\phi}_i(\mathbf{p})]^2. \tag{14}$$

3.2.3. *Optimization of codes.* In a BEM formulation for a problem involving an unknown boundary/interface, some of the matrix entries are obtained as integrals over the unknown interface. The BEM formulation leads to a system of equations, where several of the matrix entries depend on the guessed configuration of the unknown interface. In this case, eq. (9) can be partitioned as

$$\begin{bmatrix} B_{11} & B_{12}(\mathbf{p}) \\ B_{21}(\mathbf{p}) & B_{22}(\mathbf{p}) \end{bmatrix} \begin{Bmatrix} \phi_1 \\ \phi_2 \end{Bmatrix} = \begin{bmatrix} A_{11} & A_{12}(\mathbf{p}) \\ A_{21}(\mathbf{p}) & A_{22}(\mathbf{p}) \end{bmatrix} \begin{Bmatrix} \frac{\partial \phi_1}{\partial n} \\ 0 \end{Bmatrix}, \tag{15}$$

where $\mathbf{p}$ is a parameterization of the unknown internal boundaries; index 1 is associated with known boundaries and index 2 with unknown boundaries.

Because of the zero boundary condition on $\partial\phi/\partial n$ on the internal boundaries, eq. (15) shows that it is not necessary to compute the matrices A_{12} and A_{22}. Further since the matrices A_{11} and B_{11} are associated with the outer boundary, and depend only on its discretization, they need to be computed only once for a given geometry. This enables achievement of significant savings in the solution of the inverse problem. Most of the computational work that is required for the solution can be performed at the outset, and subsequent solutions of the forward problem are performed using much fewer operations. Since the minimization procedure requires solution of many forward problems with different values of the parameters, this approach results in significant speed up of the minimization.

3.2.4. *Choice of minimization technique.* Several approaches are available to minimize the quantity χ^2 in eq. (14). For problems where the error is a smooth function of the parameters, approaches that use derivative information to perform the minimization, can reach the solution much faster than those that do not.

However, they require *a priori* computation of the Jacobian. Quite often the exact Jacobian cannot be obtained analytically and an approximate Jacobian is computed by a suitable linearization process. In this case, the obtained Jacobian is only useful in the neighbourhood of the solution. Alternatively, one can use a numerical approach to compute the Jacobian by using a finite-difference approach.

For analytically computing the Jacobian a direct relationship between the measured values of the potential on the known boundaries, ϕ_1, as a function of the parameters **p**. Since, the elements of the matrices in eq. (15) are a function of the vector of parameters **p**, an explicit expression for the derivatives of the error function (Jacobian) is not readily available. In this case the Jacobians will require evaluation of tensors of third order, and is likely to prove numerically expensive. Accordingly, we have chosen in our numerical implementation to date minimization schemes that do not need analytically computed Jacobians. Three minimization algorithms that do not require analytical knowledge of the Jacobian, from Press *et al.* (1992), were accordingly chosen for testing.

The first was Nelder and Mead's downhill simplex method. In this method, an initial 'simplex' is formed by $N+1$ guesses, where N is the dimension of the minimization problem. Then, using the magnitude of the errors evaluated at the vertices of the simplex, the simplex is subjected to a sequence of stretching, reflection and contraction operations, to reduce the error at these vertices. These operations ensure that as the algorithm converges, the simplex brackets a minimum of the objective function.

The second method was Powell's direction set method. In this method, an initial guess and a set of N independent search directions are provided to the program. In each iteration, the method serially performs a sequence of line-minimizations along the directions. At the end of each iteration, the method replaces one of the original directions with the line joining the starting and ending points. Care is taken to ensure that the directions remain linearly independent.

The third method tested was the conjugate gradient method. The Jacobian was computed using finite differences. The method was tested to see if its superior convergence rate compensated for the larger number of function evaluations required by the Jacobian evaluation.

3.2.5. *Constraints on the solution.* In solving inverse problems it is quite important to constrain the solution using *a priori* information to mitigate any ill-posed character of the problem. For the present problem constraints on the geometry of the internal surfaces, or on the localized character of the distribution of σ can be formulated. However, most available non-linear multi-dimensional optimization schemes are formulated for unconstrained problems, and do not permit imposition of additional constraints. As discussed previously, our choice of the parameterization of the unknown interfaces or surfaces, introduces some of this *a priori* information in the form of the function, σ, or in the parameterization of S_{int}, without requiring specific additional constraints.

We implemented further constraints in a numerical manner by artificially modifying the error and numerical gradient calculation procedures. For example, in the case of a problem where multiple inner surfaces are to be identified, the routine that evaluates the error in the measurements was modified to return large values of the error when presented with configurations known to be wrong. These included configurations that have overlapping inner bodies, or to very large or very small sizes of the inner inclusions. In these cases the error evaluating function returns an artificially large value of the error, and an error gradient vector set to the unit vector in the direction that leads away from the error.

3.3. *Code for the EIT problem*

BEM-based numerical codes for solving the forward problem in two dimensions and three dimensions were developed. These codes were then used to synthesize EIT experimental data by simulating the measurement process for known configuration. Measurements were assumed available at each node of the BEM discretization. The forward problem codes were then embedded in an iterative minimization procedure. The codes were started with arbitrary guess configurations and the minimization procedure was used to obtain successive configurations.

4. RESULTS

4.1. *Comparison of minimization techniques*

All methods were initially tested on the imaging problem of a large cylinder containing one or many smaller inner cylindrical regions of zero conductivity. Since each of the inclusions is modelled as a circle it is parameterized by three parameters—the coordinates of its center and the radius. The methods were observed to converge very well for a variety of inner distributions of circles of varying sizes.

A systematic comparison between the three methods was conducted to choose one for further development. A specific example is shown in Figs 2 and 3. Figure 2 shows the convergence history of the Powell method. The nodes on the boundary of the exact solution are marked with open circles, the nodes on the initial guess are marked with + symbols, and the other circles are the converged solutions at the end of every Powell iteration. The other methods have similar convergence histories.

Figure 3 shows the value of the error at each function evaluation against the number of evaluations. All three methods exhibit convergence, with the downhill simplex method the fastest, followed by the Powell method, and the conjugate gradient method. The graph for the Powell method shows that as the one-dimensional minimizations are performed the code might visit points with higher errors. However, the

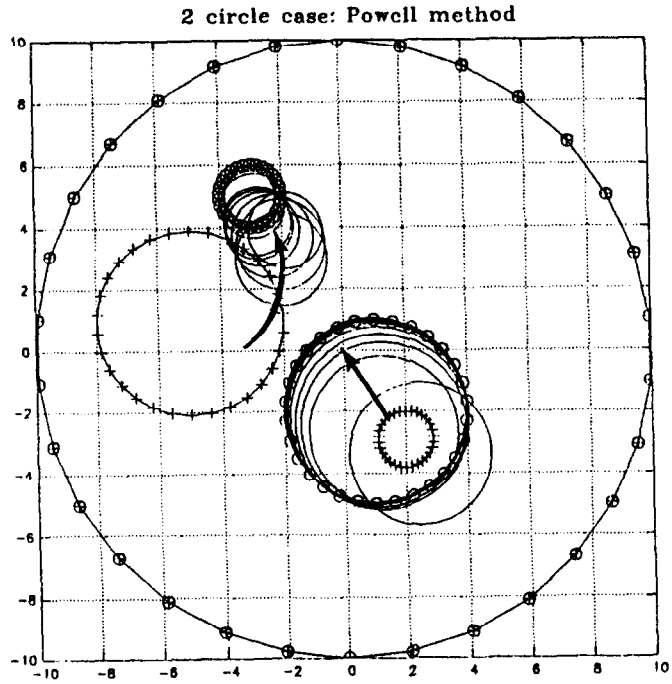

Fig. 2. Two internal regions of zero conductivity, indicated with lines with open circles, are to be imaged. The initial guess assumed is indicated with + marks. This problem was used to benchmark the three minimization methods. Also shown are the sequence of iterates for the Powell method.

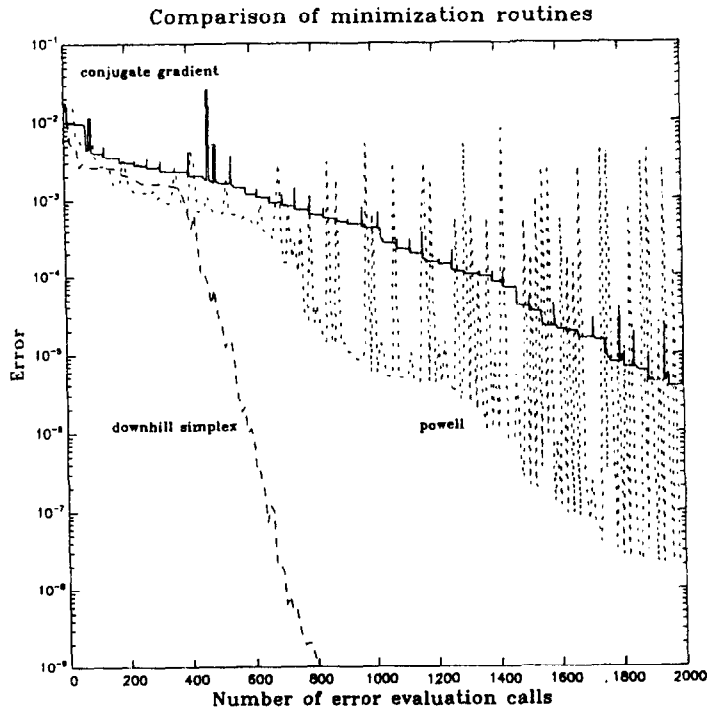

Fig. 3. Error vs the number of forward problem solutions for the downhill simplex, Powell and conjugate gradient methods for solution of the EIT inverse problem of Fig. 2.

trend of the error shows convergence. This curve would indicate that the downhill simplex method should be chosen. However, for some cases the downhill simplex method code would get stuck at a point away from the true minimum, while the Powell method appeared to be more robust and converged on all the cases considered. Accordingly, the Powell method was then employed for all subsequent evaluations.

4.2. *Identification of inclusions in two dimensions*

The method was tried on a problem in which the inner shape was arbitrary, and characterized by the location of a point, the 'center', and a set of Legendre polynomial coefficients given in eq. (10). The shape in Fig. 4 was drawn arbitrarily. As seen in the figure, the Powell method converges satisfactorily within one iteration. This takes less than a minute on our SGI Indigo workstation.

As the number of objects is increased the dimension of the parameter space in which the minimum has to be found increases, and we expect the minimization to be harder. However, we found that the Powell method is able to achieve the solutions to the problem. In Fig. 5

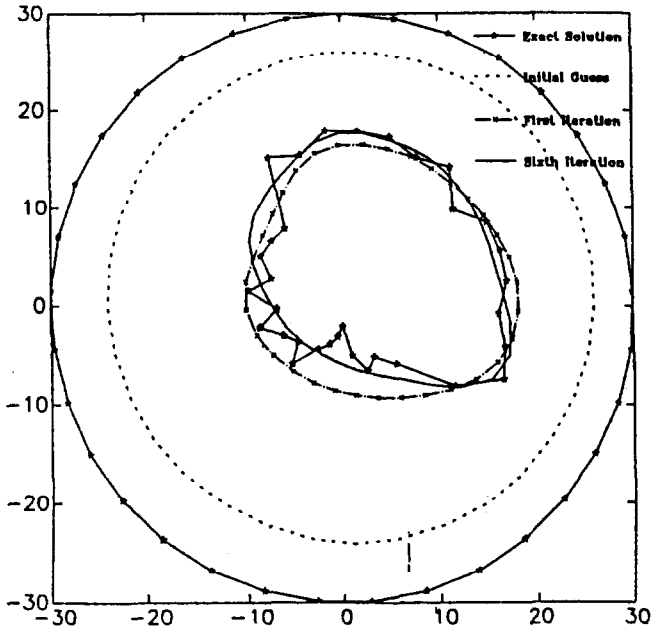

Fig. 4. EIT reconstruction of a region of zero conductivity with a jagged boundary. The inverse problem solution used a 13 parameter Legendre parametrization. Satisfactory convergence is seen, even after one iteration.

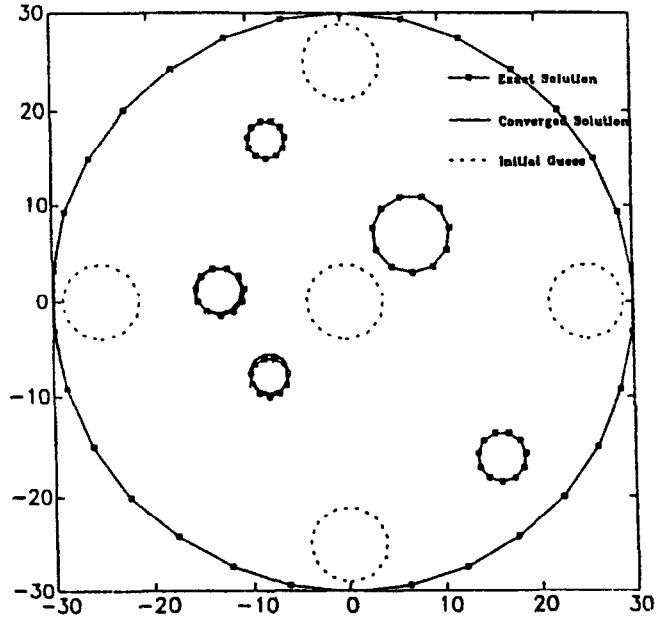

Fig. 5. EIT reconstruction of 5 circles enclosing regions of zero conductivity starting from an arbitrary guess.

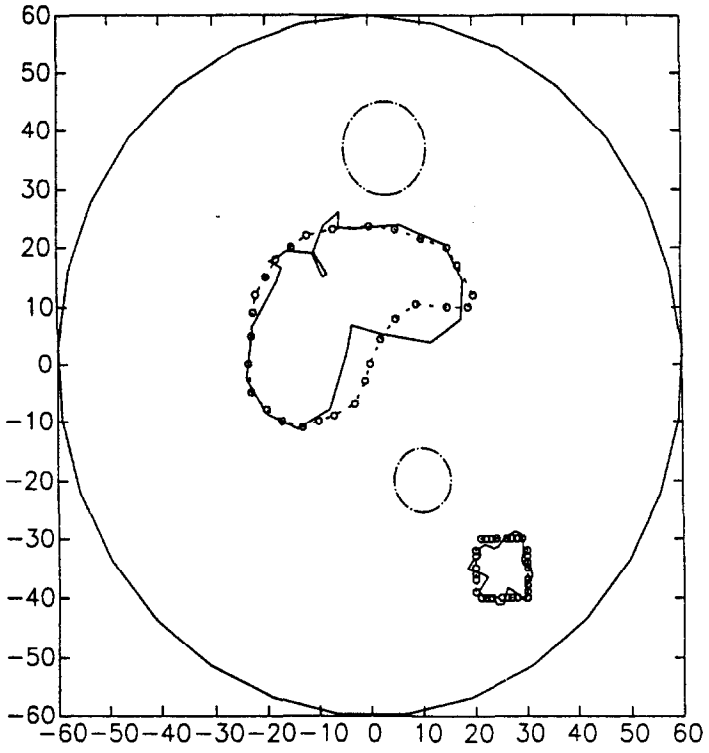

Fig. 6. EIT reconstruction of 2 arbitrary shapes (lines with open circles). A Legendre polynomial parameterization was used, even though the shapes are not well representable with such polynomials. Despite this, satisfactory convergence is observed.

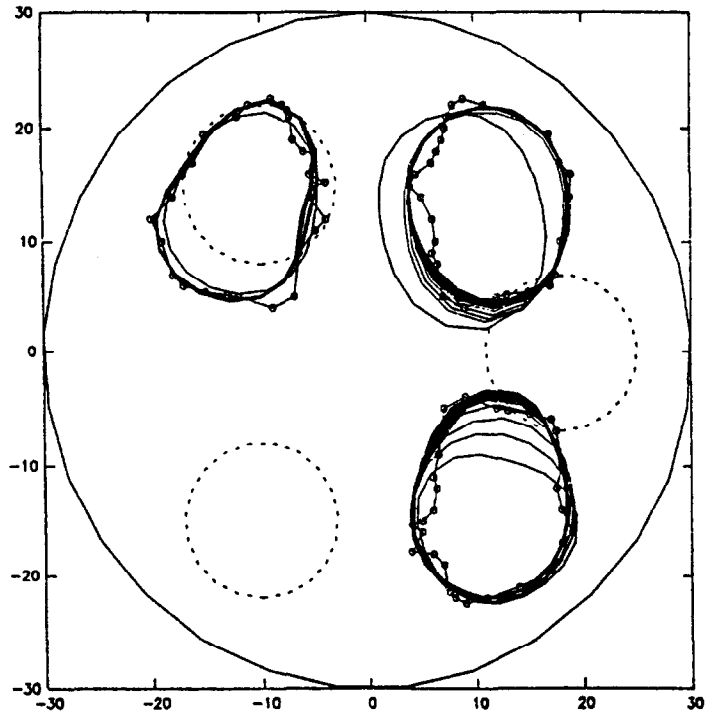

Fig. 7. EIT reconstruction of 3 arbitrary shapes using a 7-parameter Legendre parameterization. Initial guess is denoted by the dashed line, the successive iterates by solid lines, and the actual shape by the line with open circles.

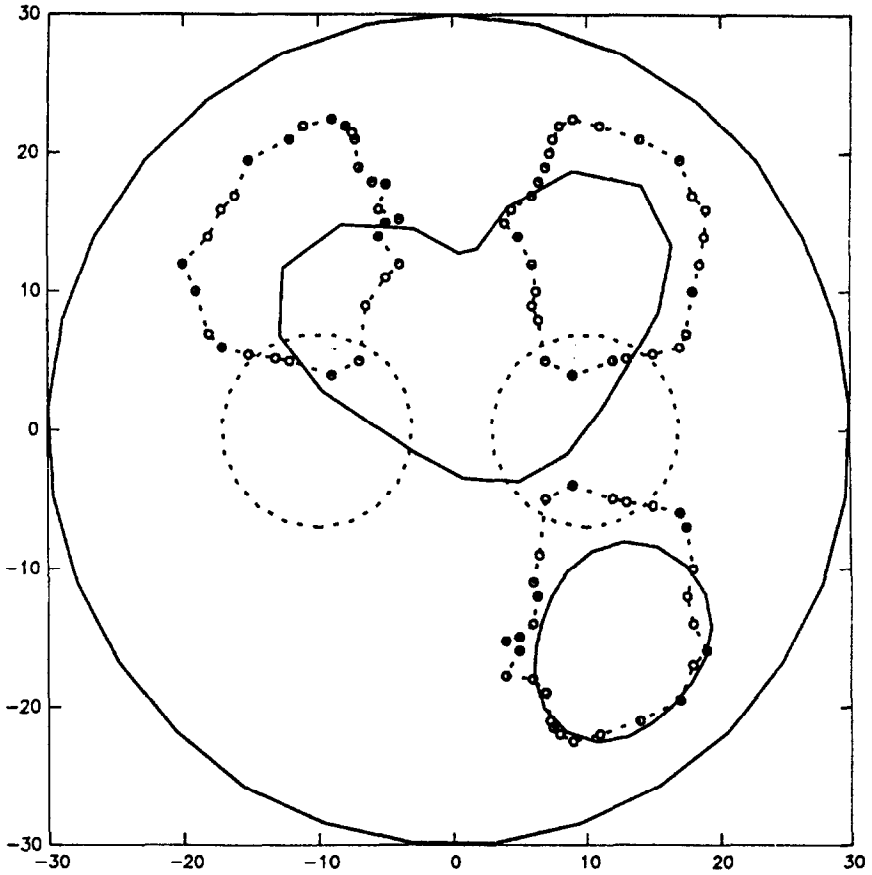

Fig. 8. EIT reconstruction of three arbitrary shapes (-o-o-) with the number of guessed shapes assumed to be two. The second computed shape spans the region occupied by two of the actual shapes (– – – initial guess, —— converged solution).

we present the result of such an inversion for five circles. An excellent convergence can be seen for an initial arbitrary guess (also shown on the figure) after about 10 iterations.

In Fig. 6 we show a further attempt at deducing two arbitrary shapes using the Powell method. Again, the shapes were entered using arbitrary freehand drawing, and their reconstruction was sought in terms of two sets of 11 Legendre polynomials. Here the Legendre polynomials cannot faithfully represent the drawn shape. However, despite this, the method achieved a satisfactory identification. Finally, Fig. 7 shows an example of three arbitrary-shaped inclusions. The reconstruction is done with 4 Legendre polynomials.

In the previous examples, the number of inclusions was assumed known in the inverse problem solution. In Fig. 8 we show a case where two inclusions are guessed while the domain contains three. The solution identified one inclusion correctly and the other two are approached by an overlapping computed shape. Figure 9 shows a converse case where the three inclusions are assumed and they approximately identified the regions occupied by the two shapes actually present. These results further emphasize the robustness and flexibility of the method that would allow it to be successful in the real imaging problems. Obviously, more work is required to include the number of inclusions in the parameters to be determined by the inverse problem solution.

4.3. *Identification of inclusions in three dimensions*

In three dimensions we sought to image regions with zero conductivity inside a larger spherical conducting region. The first example was to correctly find the position and radius of an included sphere of zero conductivity. Excellent convergence is also obtained for this case. Figure 10 shows a successful solution of a case where the radius of the outer domain is chosen to be 10, with the inside sphere of radius $R=2$ at $(3, 1, -2)$. The initial guess is $R=5$ at $(2, -3, 1)$.

Figure 11 shows a successful implementation of the code in the case where two spheres were sought. The initial guess of the spheres is shown in a cross section as the starred circles. The final shape is marked with the circle. The figure also shows the cross sections at different iteration numbers.

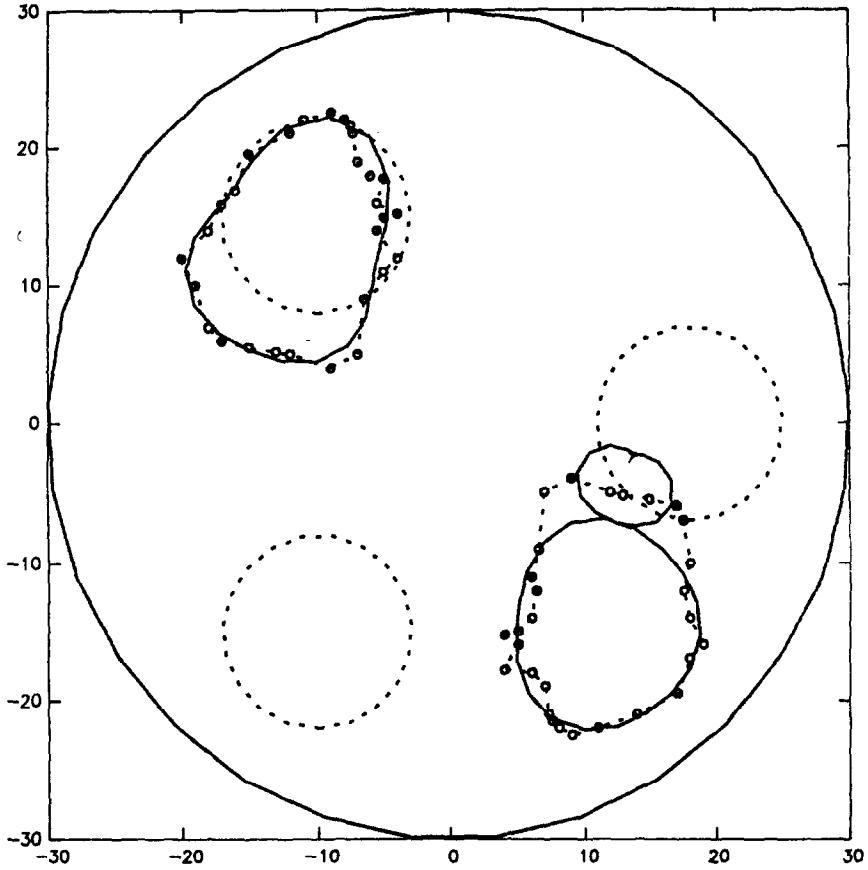

Fig. 9. EIT reconstruction of two arbitrary shapes (-o-o-) with the number of guessed shapes assumed to be three. Again, the region occupied by the actual shapes is identified by the computed shapes (– – – initial guess, —— converged solution).

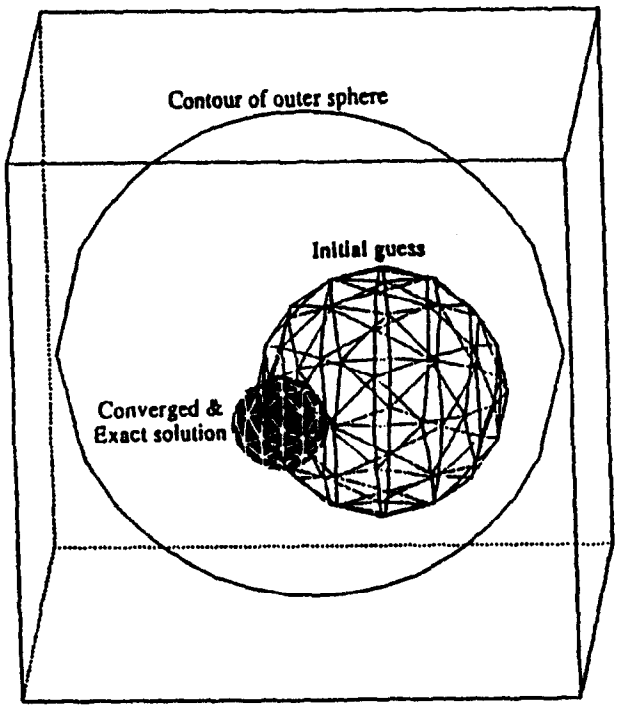

Fig. 10. EIT reconstruction in three dimensions: a spherical region of zero conductivity embedded in an outer spherical region is imaged.The initial guess and the converged solutions are shown.

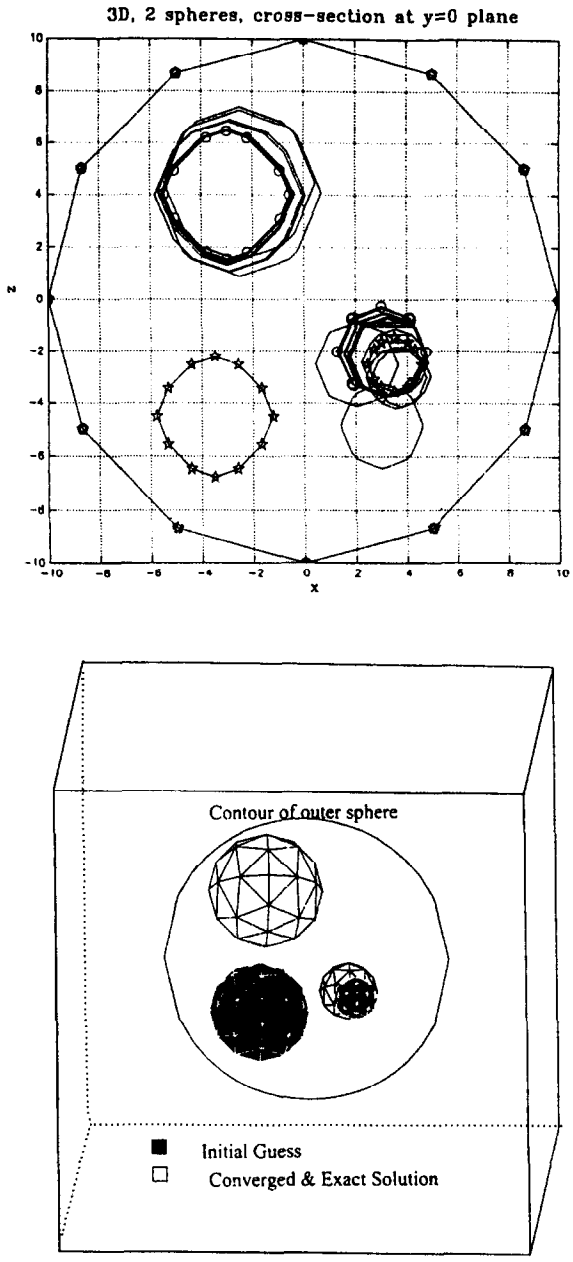

Fig. 11. Two spherical regions of zero conductivity embedded in an outer spherical region are imaged.The top figure shows a cross-sectional view with the initial guess (marked with stars), successive iterates, and the exact solution (marked with circles). A three-dimensional view of initial guess and converged solution is shown below.

5. CONCLUSIONS

This study has developed some preliminary BEM techniques for electrical impedance tomography. Computational codes for the forward problem were developed and optimized for use in the inverse problem by accounting for the fact that they would be used repeatedly with the same geometrical discretization/electrode setup but for different distributions of conductivity/inner surfaces.

A new methodology for parametrizing the unknowns of the sought impedance distribution was also developed. This decouples the parametrization of the unknown body shapes from the geometrical discretization of the problem domain, and allows the inclusion of available *a priori* information. This has the potential of mitigating the ill-posed nature of the inversion considerably. Different alternative decoupled parameterizations for the problems were developed.

The codes were then embedded in simple standard minimization schemes (downhill simplex, Powell and conjugate gradient) and found to converge to the exact distribution for many examples, e.g. for imaging

multiple circles and spheres, respectively, in two- and three-dimensions, for the identification of multiple arbitrary shapes in two-dimensions.

Acknowledgements

We would like to acknowledge helpful discussions with our colleagues at Dynaflow, Inc. The study was supported by the National Science Foundation, via grant DMI-9461681 and by Sandia National Laboratories, via contract AO-5480.

NOTATION

A, B	matrices in boundary element method
a	multiplier of angle/solid angle in BEM formulation
e	difference between measured and predicted values of the potential
E	electrode
f	a function
i, k, l	indices
M	number of electrodes
N_E	number of experiments
n, **n**	normal direction and vector
p	vector of parameters to be determined
P	number of parameters
r	radial coordinate
S	surface of boundaries enclosing the domain
x, y	position vectors
θ	angular coordinate
π	the constant
σ	conductivity
ϕ	electric potential
Ω	the domain of the problem
∇	the nabla operator

REFERENCES

Barber, B. and Brown, B. H. (1984) Applied potential tomography. *J. Phys. E. Sci. Instrum.* **17**, 723–733.

Chahine, G. L. and Duraiswami, R. (1992) Dynamical interactions in a multi-bubble cloud. *ASME J. Fluids Engng* **114**, 680–686.

Chahine, G. L. and Duraiswami, R. (1994) Boundary element method for calculating 2D and 3D underwater explosion bubble behavior in free water and near structures. White Oak Detachment Technical Report NSWCDD/TR-93/44. Naval Surface Warfare Center.

Chahine, G. L. and Perdue, T. O. (1989) A 3D boundary element method for explosion bubble dynamics. in *Drops and Bubbles*, ed. T. G. Wang, *A.I.P. Conference Prcoeedings*, Vol. 197, pp. 169–187.

Dobson, D. C. and Santosa, F. (1994) An image-enhancement technique for electrical impedance tomography. *Inverse Problems* **10**, 317–334.

Duraiswami, R., Sarkar, K., Prabhukumar, S. and Chahine, G. L. (1995) BEM methods for efficient 2D and 3D electrical impedance tomography. NSF Phase I SBIR Final Report, Grant DMI-9461681. Also, Dynaflow, Inc. Technical Report 95006-1.

Duraiswami, R., Sarkar, K. and Chahine, G. L. (1997) Efficient 2D and 3D electrical impedance tomography using dual reciprocity boundary element techniques. *Computers and Structures* (accepted).

Holder, D. (ed.) (1993) *Clinical and Physiological Applications of Electrical Impedance Tomography*. UCL Press, London, U.K.

Holder, D. and Brown, B. (eds) (1993) Biomedical applications of EIT: a critical review. In *Clinical and Physiological Applications of Electrical Impedance Tomography*. UCL Press, London, U.K.

Jones, O. C., Lin, J.-T., Shu, H., Ovacik, L. and He, Y. (1994) Impedance imaging relative to binary mixtures. In *Proceedings, Liquid Solid Flows*, 1994, eds M. C. Roco, C. T. Crowe, D. D. Joseph and E. E. Michaelides, ASME FED-Vol. 189. ASME, New York, U.S.A.

O'Hern, T. J., Torczynski, J. R., Ceccio, S. L., Tassin, A. L., Chahine, G. L., Duraiswami, R. and Sarkar, K. (1995) Development of an electrical impedance tomography system for an air–water vertical bubble column. In *Forum on Measurement Techniques in Multiphase Flows*, FED-Vol. 233, pp. 531–537. ASME, New York, U.S.A.

Press, W. H., Teukolsky, S. A., Vetterling, W. T. and Flannery, B. P. (1992) *Numerical Recipes*, 2nd Edn. Cambridge University Press, Cambridge.

Quinto, E. T., Cheney, M. and Kuchment, P. (eds) (1994) *Tomography, Impedance Imaging, and Integral Geometry*. American Mathematical Society, Providence, RI, U.S.A.

Somersalo, E., Cheney, M. and Isaacson, D. (1992) Existence and uniqueness for electrode models for electric current computed tomography. *SIAM J. Appl. Math.* **52**, 1023–1040.

Santosa, F. and Vogelius, M. (1990) A backprojection algorithm for electrical impedance imaging. *SIAM J. Appl. Math.* **50**, 216–243.

Webster, J. G. (ed.) (1990) Electrical impedance imaging. In *Electrical Impedance Tomography*. Adam Hilger, New York, U.S.A.

Yorkey, T. J., Webster, J. G. and Tompkins, W. J. (1987) Comparing reconstruction algorithms for electrical impedance tomography. *IEEE Trans. Biomedical Engng* **11**, 843–852.